

# Design, implementation, and test of skid steering-based autonomous driving controller for a robotic vehicle with articulated suspension<sup>†</sup>

Juyong Kang<sup>1</sup>, Wongun Kim<sup>2</sup>, Jongseok Lee<sup>3</sup> and Kyongsu Yi<sup>1,\*</sup>

<sup>1</sup>School of Mechanical and Aerospace Engineering, Seoul National University, Seoul, 151-742, Korea

<sup>2</sup>Program in Automotive Engineering, Seoul National University, Gwanak 599, Gwanak-ro, Gwanak-go, Seoul, Korea

<sup>3</sup>Samsung Techwin, 69-2, Sinchon-Dong, Changwon, Kyungnam-do, Korea

(Manuscript Received July 10, 2009; Revised December 24, 2009; Accepted December 29, 2009)

## Abstract

This paper describes an autonomous driving control algorithm based on skid steering for a Robotic Vehicle with Articulated Suspension (RVAS). The driving control algorithm consisted of four parts: speed controller for following the desired speed, trajectory tracking controller to track the desired trajectory, longitudinal tire force distribution algorithm which determines the optimal desired longitudinal tire force and wheel torque controller which determines the wheel torque command at each wheel to keep the slip ratio below the limit value as well as to track the desired tire force. The longitudinal and vertical tire force estimators were designed for optimal tire force distribution and wheel slip control. The dynamic model of the RVAS is validated using vehicle test data. Simulation and vehicle tests were conducted in order to evaluate the proposed driving control algorithm. Based on the simulation and test results, the proposed driving controller was shown to produce satisfactory trajectory tracking performance.

**Keywords:** Skid steering vehicle; Autonomous driving control; Trajectory tracking control; Unmanned ground vehicle

## 1. Introduction

Recently, diverse unmanned ground vehicles have been developed in order to conduct multi-tasks, such as logistics supports, surveillance, and light combat operation. In this paper, as a part of autonomous vehicle control for military or robotic vehicles, skid steering based driving control algorithm is investigated. A robotic Vehicle with Articulated Suspension (RVAS), as shown in Fig. 1, is a kind of unmanned ground vehicle based on a skid steering using independent in-wheel drive at each wheel. The RVAS, unlike the conventional wheeled vehicles, is not equipped with steering linkages. Instead, it is steered through differential traction force which is created from the in-wheel motor at each wheel. Steering in this fashion requires much more power consumption than in kinematic steering using Ackerman's linkages. However this offers a simple structure and more room in the vehicle for mission equipment installment. In the aspect of mobility, the RVAS benefits from its in-wheel drives and articulated suspensions, which provide an independent wheel traction control capability and a great improvement in obstacle negotiation ability, respectively. [1, 2]

The proposed driving control algorithm is related to motion control of skid steering vehicle and trajectory tracking control. Diverse control strategies for skid steering vehicle were proposed through previous research. Suresh presented the steering controller of a six-wheeled vehicle based on skid steering. The steering controller consists of a proportional-integral-derivative (PID) controller with two filters, a prediction filter and a safety filter [3]. Economou and Colyer proposed fuzzy logic control of wheeled skid-steer electric vehicles [4]. Dixon *et al.* investigated nonlinear control of wheeled mobile robots [5]. Also, research related to trajectory tracking has been conducted for a few decades. Kang *et al.* designed and tested a controller for autonomous vehicle path tracking using GPS/INS sensors [6]. Peng proposed a path tracking controller based on the optimal finite preview control method [7]. However since research was conducted for a conventional suspension vehicle, the articulated suspension vehicle, such as the



Fig. 1. Robotic Vehicle with Articulated Suspension (RVAS).

<sup>†</sup> This paper was recommended for publication in revised form by Associate Editor Moon Ki Kim

\*Corresponding author. Tel.: +82 2 880 1941, Fax.: +82 2 880 1942

E-mail address: kyi@snu.ac.kr

© KSME & Springer 2010

RVAS, is not applicable.

In this paper, the driving control algorithm based on skid steering of RVAS is investigated in order to track a prescribed trajectory. Simulation and vehicle tests are conducted in order to evaluate the proposed driving controller.

## 2. Vehicle dynamic model

The vehicle dynamic model was developed using “Matlab Simulink” in order to conduct numerical simulation studies [2]. The full dynamic model of the RVAS was designed with three parts: driving system, arm dynamic model, and vehicle body dynamic model as shown in Fig. 2. The driving system contains an in-wheel motor model, a wheel dynamic model, and a tire model. The arm dynamic model determines the dynamic behaviors of the *i*-th arm rod. The vehicle body dynamic model was designed to represent the dynamic behavior of a sprung mass.

The in-wheel motor was modeled using a first order transfer function and the torque/speed curve as shown in Fig. 3 was considered. Longitudinal and lateral tire models were modeled using a combined Pacejka tire model [7].

The arm dynamic model determines the arm behavior of each arm rod and internal forces and moments acting on a sprung mass. The arm behavior is occurred from longitudinal, lateral and vertical tire forces and arm spring and damping

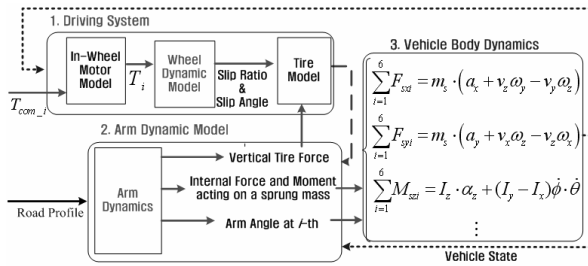


Fig. 2. Vehicle dynamic model.

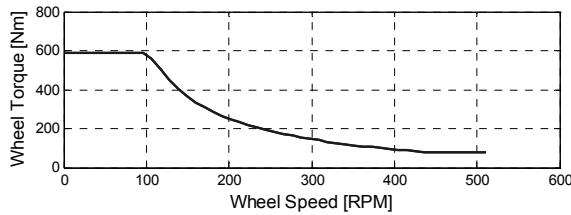


Fig. 3. Torque/speed curve of each in-wheel motor.

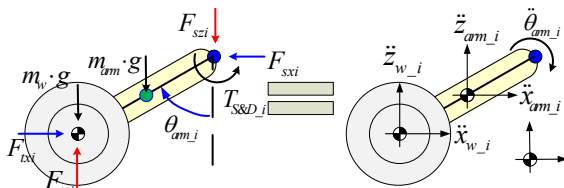


Fig. 4. Dynamic equilibrium of *i*-th arm rod.

torques. Fig. 4 shows the dynamic equilibrium of the *i*-th arm rod.

From Fig. 4, the dynamic equations for the arm dynamic model can be obtained as follows:

$$\begin{aligned} \sum F_x &= F_{txi} - F_{sxi} = m_{arm} \cdot \ddot{x}_{arm\_i} + m_w \cdot \ddot{x}_{w\_i} \\ \sum F_y &= F_{tyi} - F_{syi} = m_{arm} \cdot \ddot{y}_{arm\_i} + m_w \cdot \ddot{y}_{w\_i} \\ \sum F_z &= F_{tzi} - F_{szi} - (m_w + m_{arm}) \cdot g = m_{arm} \cdot \ddot{z}_{arm\_i} + m_w \cdot \ddot{z}_{w\_i} \end{aligned} \quad (1)$$

$$\begin{aligned} \sum M_x &= \left\{ I_{arm\_x} \cdot \alpha_{arm\_x} + (I_{arm\_z} - I_{arm\_y}) \cdot \omega_{arm\_y} \cdot \omega_{arm\_z} \right. \\ &\quad \left. + l_{arm} \cdot \cos(\theta_{arm\_i}) \cdot (m_w \cdot \ddot{y}_{wi} + m_{arm} \cdot \ddot{y}_{arm\_i} / 2) \right\} \\ \sum M_y &= \left\{ I_{arm\_y} \cdot \alpha_{arm\_y} + (I_{arm\_z} - I_{arm\_x}) \cdot \omega_{arm\_z} \cdot \omega_{arm\_x} \right. \\ &\quad \left. - (m_w \cdot \ddot{x}_{wi} + m_{arm} \cdot \ddot{x}_{arm\_i} / 2) \cdot l_{arm} \cdot \cos(\theta_{arm\_i}) \right. \\ &\quad \left. + (m_w \cdot \ddot{z}_{wi} + m_{arm} \cdot \ddot{z}_{arm\_i} / 2) \cdot l_{arm} \cdot \sin(\theta_{arm\_i}) \right\} \\ \sum M_z &= \left\{ I_{arm\_z} \cdot \alpha_{arm\_z} + (I_{arm\_y} - I_{arm\_x}) \cdot \omega_{arm\_x} \cdot \omega_{arm\_y} \right. \\ &\quad \left. - l_{arm} \cdot \sin(\theta_{arm\_i}) \cdot (m_w \cdot \ddot{y}_{wi} + m_{arm} \cdot \ddot{y}_{arm\_i} / 2) \right\} \end{aligned} \quad (2)$$

In Eqs. (1) and (2), the rotational accelerations of the arm rod and the translational accelerations of the *i*-th wheel are given and further shown in Eqs. (3) and (4):

$$\begin{aligned} \alpha_{arm} &= [\alpha_{arm\_x} \quad \alpha_{arm\_y} \quad \alpha_{arm\_z}]^T = \alpha_{ch} + \alpha_{arm/ch} + \omega_{ch} \times \omega_{arm/ch} \\ &= \begin{bmatrix} \dot{\phi} \\ \ddot{\theta} \\ \dot{\phi} \end{bmatrix} + \begin{bmatrix} 0 \\ \ddot{\theta}_{arm\_i} \\ 0 \end{bmatrix} + \begin{bmatrix} \dot{\phi} \\ \dot{\theta} \\ \dot{\phi} \end{bmatrix} \times \begin{bmatrix} 0 \\ \dot{\theta}_{arm\_i} \\ 0 \end{bmatrix} = \begin{bmatrix} \ddot{\phi} - \dot{\theta}_{arm\_i} \cdot \dot{\phi} \\ \ddot{\theta} + \dot{\theta}_{arm\_i} \\ \ddot{\phi} + \dot{\theta}_{arm\_i} \cdot \dot{\phi} \end{bmatrix} \end{aligned} \quad (3)$$

$$\begin{aligned} \ddot{r}_{wi} &= [\ddot{x}_{wi} \quad \ddot{y}_{wi} \quad \ddot{z}_{wi}]^T = \ddot{r}_i + \omega_{arm} \times [\omega_{arm} \times r_{wi}] + \alpha_{arm} \times r_{wi/i} \\ \ddot{r}_i &= [\ddot{x}_i \quad \ddot{y}_i \quad \ddot{z}_i]^T = \ddot{r}_{cg} + \omega_{ch} \times [\omega_{ch} \times r_{i/cg}] + \alpha_{ch} \times r_{i/cg} \end{aligned} \quad (4)$$

Also, the moment summations in Eq. (2) are shown in the following:

$$\begin{cases} \sum M_x = -M_{sxi} + l_{arm} \cdot \cos(\theta_{arm\_i}) \cdot F_{tyi} \\ \sum M_y = \left\{ -T_{S\&D\_i} - l_{arm} \cdot \sin(\theta_{arm\_i}) \cdot (m_w + m_{arm} / 2) \cdot g \right\} \\ \sum M_z = -M_{szi} - T_{self} - l_{arm} \cdot \sin(\theta_{arm\_i}) \cdot F_{tyi} \end{cases} \quad (5)$$

where  $T_{S\&D\_i}$  denotes the sum of the spring and damping torques of the *i*-th arm rod:

$$T_{S\&D}(\theta_{arm\_i}, \dot{\theta}_{arm\_i}) = -k_s \cdot \theta_{arm\_i} - c_d \cdot \dot{\theta}_{arm\_i} \quad (6)$$

Substituting Eqs. (3) and (4) into Eq. (2), the dynamic equation for the arm motion can be obtained as follows:

$$\{ I_{arm\_y} + (m_w + m_{arm} / 4) \cdot l_{arm}^2 \} \cdot \ddot{\theta}_{arm\_i} =$$

$$\left\{ \begin{aligned} &\sum M_y - \{I_{arm\_y} + (m_w + m_{arm}/4) \cdot I_{arm}^2\} \cdot \ddot{\theta} - (I_{arm\_x} - I_{arm\_z}) \cdot \dot{\phi} \cdot \dot{\phi} \\ &+ (m_w + m_{arm}/2) \cdot I_{arm} \cdot \{\cos(\theta_{arm\_i}) \cdot \ddot{x}_i - \sin(\theta_{arm\_i}) \cdot \ddot{z}_i\} \\ &- (m_w + m_{arm}/4) \cdot I_{arm}^2 \cdot \sin(\theta_{arm\_i}) \cdot \cos(\theta_{arm\_i}) \cdot (\dot{\phi}^2 - \dot{\phi}^2) \\ &- (m_w + m_{arm}/4) \cdot I_{arm}^2 \cdot \{\cos^2(\theta_{arm\_i}) - \sin^2(\theta_{arm\_i})\} \cdot \dot{\phi} \cdot \dot{\phi} \end{aligned} \right\} \quad (7)$$

As a result, using the arm motion obtained from Eq. (7), the internal forces and moments acting on the sprung mass can be calculated from Eqs. (1) and (2). Finally, the motion of the sprung mass can be calculated from the internal forces and moments using the d'Alembert's principle [7].

Validation of the vehicle dynamic model was conducted by comparison of simulation results to test data of the RVAS. The driving control algorithm that was implemented in the vehicle test was used identically in the dynamic model simulation. The desired speed obtained from the vehicle test was used in the simulation.

Fig. 5 shows a comparison of test data and simulation results. The simulation results are quite identical to the test data, except for the yaw rate. The difference between the test data and the simulation results is from the vertical road profile and an offset of the mass center of the test platform. In the case of the vehicle test, the yaw rate was fluctuated by the road profile.

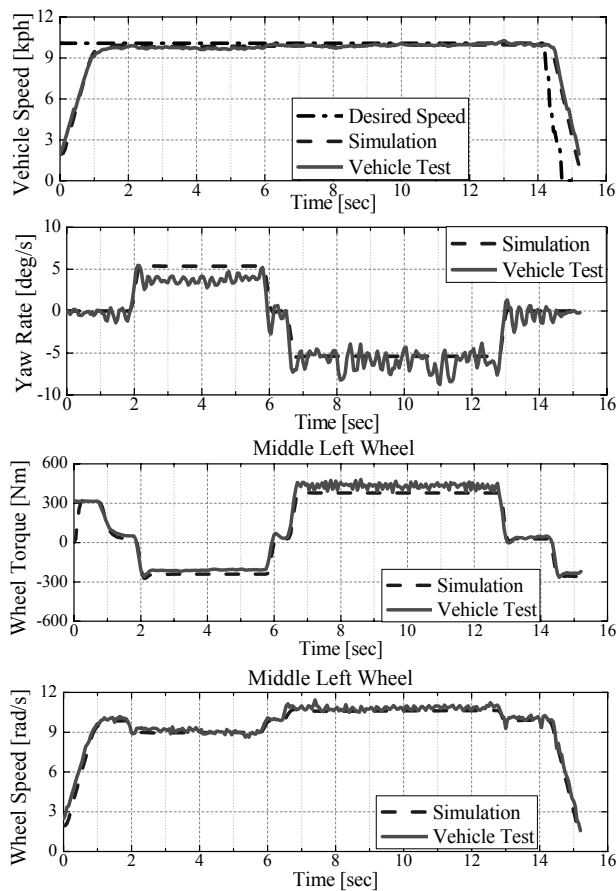


Fig. 5. Comparison of test data and simulation results.

Also, the offset of the mass center caused the left yaw motion to be smaller than the right yaw motion in an identical yaw motion command. However the simulation results agree generally with the test data, suggesting that the designed dynamic model is feasible as a test platform for development of the driving controller.

### 3. Controller design

Fig. 6 shows a control strategy of the driving controller based on a skid steering. Since it is difficult to determine the wheel torque command directly, the driving control algorithm for the RVAS was designed with four parts as follows; speed controller, trajectory tracking controller, tire force distribution algorithm, and wheel torque controller.

A schematic diagram of the proposed driving control algorithm is shown in Fig. 7. The speed controller in the upper-level controller was designed to follow the desired speed using the PI control method [6]. The trajectory tracking controller determines the yaw moment input in order to track the desired trajectory. The total traction force and the yaw moment input, upper level control inputs, should be applied to the RVAS through the longitudinal tire force distribution algorithm and wheel torque controller. Therefore, the objective of the tire force distribution algorithm is to determine how much force is required at each wheel. The desired longitudinal tire force of each wheel was determined in proportion to the vertical tire force. The wheel torque controller computes the wheel torque command in order to track the desired longitudinal tire force and at the same time to keep the slip ratio below the limit value. Additionally, the longitudinal and vertical tire force estimators are required for optimal tire force distribution and wheel slip control [2, 8-10].

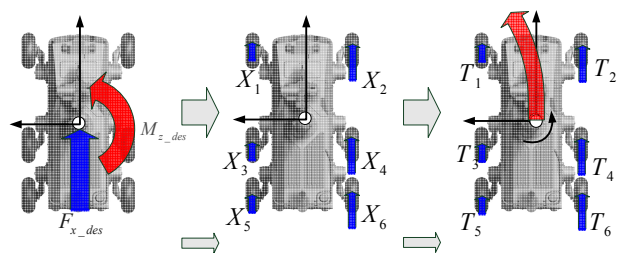


Fig. 6. Control strategy of the driving controller.

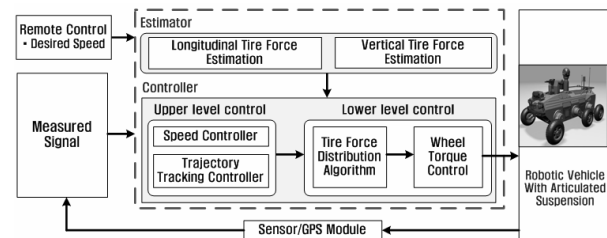


Fig. 7. Block diagram of autonomous driving control algorithm based on a skid steering.

3.1 Upper level controller

The upper level controller in the driving control algorithm consisted of the speed controller and the trajectory tracking controller. The trajectory tracking controller determines the yaw moment input for tracking the desired trajectory. The trajectory tracking controller was designed based on an optimal finite preview control method, as shown in Fig. 8.

In Fig. 8, the lateral position error,  $y_r$  is defined as the lateral distance between the vehicle center of gravity (C) and the center-line of the desired trajectory (R). The yaw angle error,  $\varphi - \varphi_d$ , is defined using the yaw angle of the vehicle and the desired yaw angle as dictated by the desired trajectory. The rate of change in the lateral position error and yaw angle error are defined as in Eqs.(8) and (9):

$$\Delta y_r = v_y \cdot \Delta t + v_x \cdot \Delta t \cdot (\varphi - \varphi_d) \tag{8}$$

$$\dot{y}_r = v_y + v_x \cdot (\varphi - \varphi_d)$$

$$\Delta \varphi_d = \frac{v_x \cdot \Delta t}{\rho} \Rightarrow \dot{\varphi}_d = \frac{v_x}{\rho} \tag{9}$$

where  $\rho$  is the curvature radius of the desired trajectory.

We seek to eliminate the lateral and yaw angle error through a combination of feedback and feed-forward control. The feedback control input of the trajectory tracking controller was computed using the lateral position error and yaw angle error. The feed-forward control input was computed using the road information within the preview distance,  $L_p$ . To develop the trajectory tracking controller using the finite preview control theory, preview distance was transformed into preview time,  $T_p$ , as in Eq. (10):

$$T_p = \frac{L_p}{v_x} \tag{10}$$

A 2-DOF bicycle model modified in view of skid steering vehicle was used to design the trajectory tracking controller, as shown in Fig. 9. Eq. (11) represents the dynamic equation of the modified bicycle model:

$$\begin{aligned} m \cdot (\dot{v}_y + v_x \cdot \dot{\varphi}) &= 2 \cdot F_{yf} + 2 \cdot F_{ym} + 2 \cdot F_{yr} \\ I_z \cdot \dot{\varphi} &= l_f \cdot F_{yf} - l_m \cdot F_{ym} - l_r \cdot F_{yr} + M_{z\_des} \end{aligned} \tag{11}$$

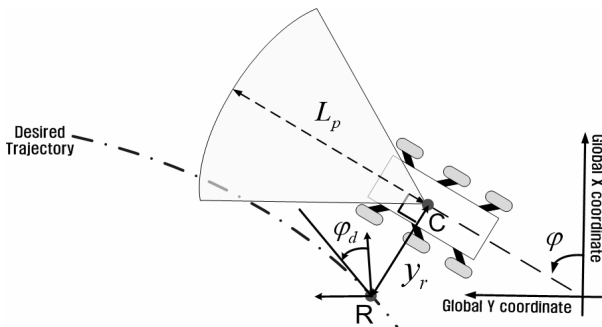


Fig. 8. Trajectory tracking controller.

From the linear tire model and Eqs.(8) and (9), the lateral tire forces can be represented as follows:

$$\begin{aligned} F_{yf} &= C_f \cdot \left\{ -\frac{\dot{y}_r + l_f \cdot (\dot{\varphi} - \dot{\varphi}_d)}{v_x} + (\varphi - \varphi_d) - \frac{l_f}{v_x} \cdot \dot{\varphi}_d \right\} \\ F_{ym} &= C_m \cdot \left\{ -\frac{\dot{y}_r - l_m \cdot (\dot{\varphi} - \dot{\varphi}_d)}{v_x} + (\varphi - \varphi_d) + \frac{l_m}{v_x} \cdot \dot{\varphi}_d \right\} \\ F_{yr} &= C_r \cdot \left\{ -\frac{\dot{y}_r - l_r \cdot (\dot{\varphi} - \dot{\varphi}_d)}{v_x} + (\varphi - \varphi_d) + \frac{l_r}{v_x} \cdot \dot{\varphi}_d \right\} \end{aligned} \tag{12}$$

where  $C_f$ ,  $C_m$  and  $C_r$  denote the equivalent front, middle and rear cornering stiffnesses. Substituting Eq. (12) into Eq. (11), the state equations for the design of the tracking controller can be obtained as in Eq. (13):

$$\begin{aligned} \dot{x} &= A \cdot x + B \cdot M_{z\_des} + F_d \cdot w_d \\ x &= [y_r \quad \dot{y}_r \quad \varphi - \varphi_d \quad \dot{\varphi} - \dot{\varphi}_d]^T \end{aligned} \tag{13}$$

where

$$\begin{aligned} A &= \begin{bmatrix} 0 & 1 & 0 & 0 \\ 0 & \frac{A_1}{v_x} & -A_1 & \frac{A_2}{v_x} \\ 0 & 0 & 0 & 1 \\ 0 & \frac{A_3}{v_x} & -A_3 & \frac{A_4}{v_x} \end{bmatrix} & B &= \begin{bmatrix} 0 \\ 0 \\ 0 \\ \frac{1}{I_z} \end{bmatrix} & F_d &= \begin{bmatrix} 0 & 0 \\ 1 & 0 \\ 0 & 0 \\ 0 & 1 \end{bmatrix} & w_d &= \begin{bmatrix} d_1 \\ d_2 \end{bmatrix} \\ A_1 &= \frac{2 \cdot (C_f + C_m + C_r)}{m} & A_2 &= -\frac{2(l_f^2 \cdot C_f + l_m^2 \cdot C_m + l_r^2 \cdot C_r)}{I_z} \\ A_3 &= \frac{2 \cdot (l_f \cdot C_f - l_m \cdot C_m - l_r \cdot C_r)}{m} & d_1 &= -v_x \cdot \dot{\varphi}_d + \frac{A_2}{v_x} \cdot \dot{\varphi} \\ A_4 &= \frac{2 \cdot (l_f \cdot C_f - l_m \cdot C_m - l_r \cdot C_r)}{I_z} & d_2 &= \frac{A_1}{v_x} \cdot \dot{\varphi}_d - \dot{\varphi}_d \end{aligned}$$

In this study, the yaw moment input was determined using the optimal finite preview control method. The yaw moment input consists of a feedback control input,  $-K_{opt} \cdot x(t)$ , and a feed-forward control input,  $M_{pre}$ , as in Eq. (14). [6, 11]:

$$M_{z\_des}(t) = -K_{opt} \cdot x(t) + M_{pre}(t) \tag{14}$$

The feedback gain in Eq. (14) can be obtained from the control algebraic Riccati equation, and the feedforward input can be computed as in Eq. (15).

$$M_{pre}(t) = -R^{-1} \cdot B^T \cdot \left[ \begin{array}{c} \int_0^{T_p} e^{A_c^T \cdot \tau} \cdot P_{ss} \cdot F_d \cdot w(t + \tau) \cdot d\tau \\ -(A_c^T)^{-1} \cdot e^{A_c^T \cdot T_p} \cdot P_{ss} \cdot F_d \cdot w_d(t + T_p) \end{array} \right] \tag{15}$$

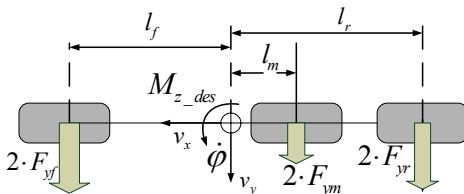


Fig. 9. Modified 2-DOF bicycle model.

where  $A_c = A - B \cdot R^{-1} \cdot B^T \cdot P_{ss}$  and  $P_{ss}$  denotes the solution of the control algebraic Riccati equation. From Eq. (15), it is clear that the yaw moment input was computed using the desired trajectory information between  $t$  and  $t + T_p$ .

### 3.2 Tire force distribution algorithm

In the previous section, the upper level control inputs were determined. The upper level control inputs should be determined to the test platform through the tire force distribution. Therefore, the objective of the tire force distribution algorithm is to compute how much force should be generated at each wheel. From the concept of friction circle, it is well known that the magnitude of the tire force acting on a tire is proportional to the vertical tire force. Using this concept and to simplify the optimization problem as well as to obtain a linear equation system, the cost function in Eq. (16) is chosen in order to obtain the desired longitudinal tire force at each wheel [12]:

$$J_{cost} = \sum_{i=1}^6 \left( W_i \cdot \frac{X_i^2}{\hat{F}_{zi}^2} \right) \quad (16)$$

where  $W_i$  denotes the weighting coefficient at the  $i$ -th wheel. The desired tire forces have to satisfy the constraints in Eqs. (17) and (18) in order to generate the total traction force input and the yaw moment input:

$$F_{x\_des} = X_1 + X_2 + X_3 + X_4 + X_5 + X_6 \quad (17)$$

$$M_{z\_des} = -t_w \cdot [(X_1 - X_2) + (X_3 - X_4) + (X_5 - X_6)] \quad (18)$$

Substituting Eqs. (17) and (18) into Eq. (16), the cost function of Eq. (16) is not subjected to any constraints, and its optimum can be found as shown in Eq. (19):

$$\begin{aligned} \frac{\partial J_{cost}}{\partial X_1} = 0 &= \frac{2W_1}{\hat{F}_{z1}} \cdot X_1 - \frac{2W_5}{\hat{F}_{z5}} \cdot \left[ \frac{F_{x\_des}}{2} - \frac{M_{z\_des}}{2t_w} - X_1 - X_3 \right] \\ \frac{\partial J_{cost}}{\partial X_2} = 0 &= \frac{2W_2}{\hat{F}_{z2}} \cdot X_2 - \frac{2W_6}{\hat{F}_{z6}} \cdot \left[ \frac{F_{x\_des}}{2} + \frac{M_{z\_des}}{2t_w} - X_2 - X_4 \right] \\ \frac{\partial J_{cost}}{\partial X_3} = 0 &= \frac{2W_3}{\hat{F}_{z3}} \cdot X_3 - \frac{2W_5}{\hat{F}_{z5}} \cdot \left[ \frac{F_{x\_des}}{2} - \frac{M_{z\_des}}{2t_w} - X_1 - X_3 \right] \\ \frac{\partial J_{cost}}{\partial X_4} = 0 &= \frac{2W_4}{\hat{F}_{z4}} \cdot X_4 - \frac{2W_6}{\hat{F}_{z6}} \cdot \left[ \frac{F_{x\_des}}{2} + \frac{M_{z\_des}}{2t_w} - X_2 - X_4 \right] \end{aligned} \quad (19)$$

### 3.3 Wheel torque controller

The aim of the RVAS is to drive on a variety of rough terrains. Also, it is difficult to obtain the complete characteristics of the longitudinal tire force according to the driving condition. Therefore, it is assumed that the characteristic of the longitudinal tire force is unknown in designing the wheel torque controller.

The wheel torque controller is designed to keep the slip ra-

tio of each wheel below the limit value,  $\lambda_{max}$ , as well as to track the desired longitudinal tire force. In the case of a sufficiently small slip ratio, the wheel torque command can be determined as in Eq. (20) in order to track the desired longitudinal tire force:

$$T_{com\_i}(k) = R_i \cdot X_i(k) \quad (20)$$

However this control input may cause the deviation of the wheel slip ratio when the wheel is lifted-off or excessive longitudinal tire force is required. In this study, when the wheel slip ratio was larger than the limit value, the wheel torque controller was designed so that the actual wheel speed tracks the desired wheel speed. The desired wheel speed is represented as follows [13]:

$$\omega_d = \begin{cases} \frac{V_i}{R_i \cdot (1 - \lambda_{max})} & \text{if } (\lambda > \lambda_{max}) \\ \frac{V_i}{R_i} \cdot (1 - \lambda_{max}) & \text{if } (\lambda < -\lambda_{max}) \end{cases} \quad (21)$$

where  $V_i$  denotes the longitudinal velocity at the  $i$ -th wheel. The wheel torque command for tracking the desired wheel speed was obtained based on the sliding mode control method and wheel dynamics as follows:

$$\begin{aligned} s_w = \omega_d(k) - \omega_i(k), \quad \frac{1}{2} \frac{d}{dt} s_w^2 = s_w \cdot \dot{s}_w = -K_w |s_w| \\ \dot{s}_w = -\dot{\omega}_i = -\frac{1}{J_w} \{ T_{com\_i}(k) - R_i \cdot \hat{F}_{zi}(k) \} = -K_w \cdot \text{sgn}(s_w) \end{aligned} \quad (22)$$

where  $K_w$  is a positive constant. As a result, the wheel torque command can be determined as shown in Eq. (23).

$$T_{com\_i}(k) = \begin{cases} R_i \cdot X_i(k) & \text{if } (|\lambda| < \lambda_{max}) \\ R_i \cdot \hat{F}_{zi}(k) + J_w \cdot K_w \cdot \text{sat}(s_w / \Phi_w) & \text{if } (|\lambda| \geq \lambda_{max}) \end{cases} \quad (23)$$

where  $\Phi_w$  denotes the boundary condition of the saturation function.

## 4. Vehicle test results

The tests were performed using the control system shown in Fig. 10. The control system consisted of a remote control module, an actuator system and a sensor system. The remote

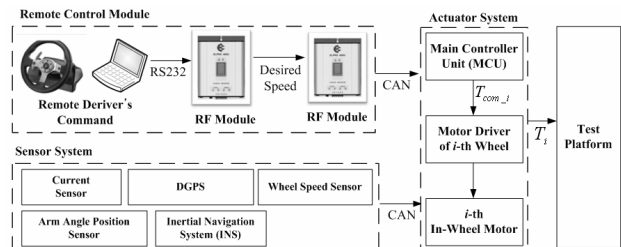
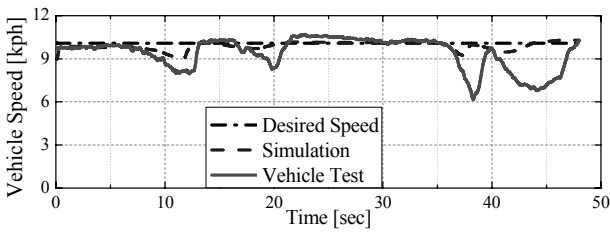
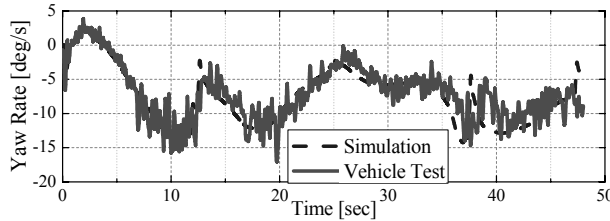


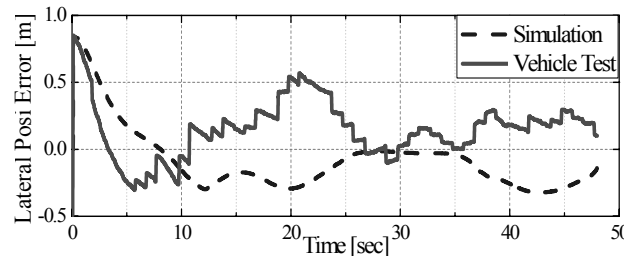
Fig. 10. Configuration of the control system.



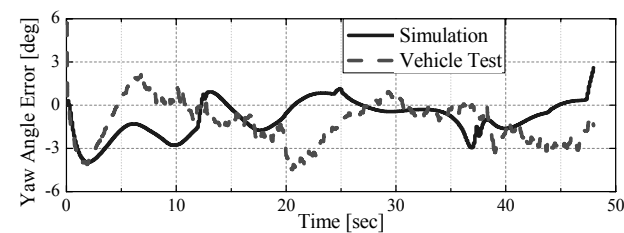
(a) Vehicle speed [kph]



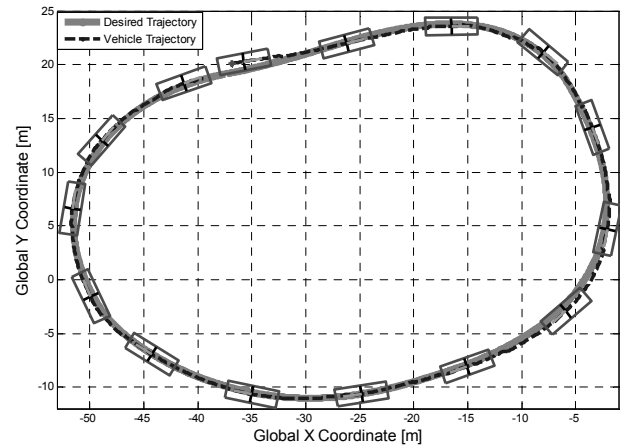
(b) Vehicle yaw rate [deg/s]



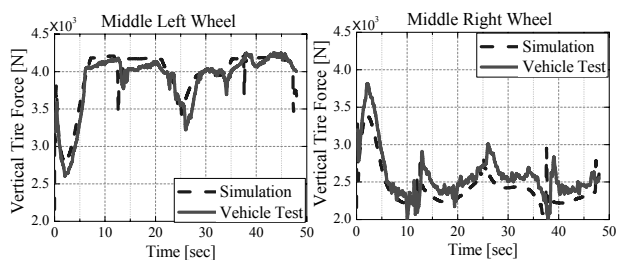
(c) Lateral position error [m]



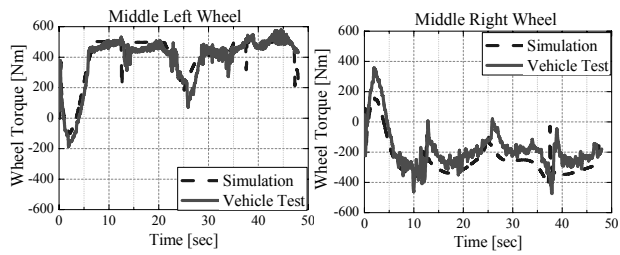
(d) Yaw angle error [deg]



(e) Desired trajectory and vehicle trajectory



(f) Estimated vertical tire force of middle wheel [N]



(g) Middle wheel torque [Nm]

Fig. 11. Comparison of the simulation and test results.

control module is used to communicate the remote driver’s command to the main controller unit. The driving controller was implemented. The ADTM-C6713 DSP module was used as the main controller unit. The motor driver in the actuator system determines the current input to needed for wheel torque command at each wheel. In the actuator system, the rated output of in-wheel motor was 5 kW. The vehicle state was measured using an inertial navigation system, a differential global positioning system, a current sensor, a wheel speed sensor, and an arm position sensor. The entire control loop shown in Fig. 10 was closed at 100 Hz.

The vehicle test results are presented in Fig. 11. The vehicle tests were compared with the simulation results, as shown in Fig. 11. Fig. 11(a) denotes the speed control performance. In this test, the desired speed was set to be 10 km/h. In the case

of the vehicle test, the speed control performance decreased due to the maximum wheel torque of the in-wheel motor, as shown in Fig. 11(a). The actual yaw rate in the vehicle test agrees closely with the simulation results, as shown in Fig. 11(b). The trajectory tracking performance is presented in Figs. 11(c) and 11(d). From these figures, it can be confirmed that the proposed trajectory tracking controller produced satisfactory tracking performance, with the magnitudes of the lateral and yaw angle errors below 0.5 m and 3.0°, respectively. These errors are the same order of magnitude as the errors predicted in the simulation. Fig. 11(e) shows the desired trajectory and vehicle position obtained using DGPS. Finally, the wheel torque input was determined in proportion to the estimated vertical tire force, as shown in Figs. 11(f) and 11(g).

## 5. Conclusions

In this paper, the skid steering based autonomous driving controller for RVAS was presented. A vehicle model for numerical simulation study was developed and validated using test data. From the simulation and test results, the proposed driving controller was found to compute the suitable wheel torque command to track the desired speeds and the desired trajectory. For optimal tire force distribution, the vertical tire force was estimated from the measured wheel speed using wheel dynamics and arm dynamics. The proposed driving controller can provide satisfactory trajectory tracking performance.

## Acknowledgment

This work has been supported by the Samsung Techwin, the BK 21 Program, the SNU-IAMD, the Korea Research Foundation Grant funded by the Korean Government (MEST) (KRF-2009-200-D00003), National Research Foundation of Korea Grant funded by the Korean Government (2009-0083495) and the Agency to Defense Development.

## Nomenclature

$g$	: Gravity acceleration
$l_f$	: Distance from center of gravity(C.G.) to front wheel axle
$l_m$	: Distance from C.G to middle wheel axle
$l_r$	: Distance from C.G to rear wheel axle
$t_w$	: Tread (track width)
$l_{arm}$	: Length of arm rod
$m$	: Vehicle mass
$m_w$	: Mass of in-wheel motor
$m_{arm}$	: Mass of arm rod
$I_z$	: Moment of inertia of the vehicle about the yaw axis
$J_w$	: Moment of inertia of in-wheel motor
$I_{arm\_x}$	:Moment of inertia of the arm rod about the roll axis
$I_{arm\_y}$	:Moment of inertia of the arm rod about the pitch axis
$I_{arm\_z}$	:Moment of inertia of the arm rod about the yaw axis
$R_i$	: Tire radius of i-th wheel
$v_x$	: Vehicle longitudinal velocity
$v_y$	: Vehicle lateral velocity
$\dot{\phi}$	: Roll rate
$\dot{\theta}$	: Pitch rate
$\dot{\psi}$	: Yaw rate
$\theta_{arm\_i}$	: Arm angle of i-th arm rod
$\omega_i$	: Wheel angular speed of i-th wheel
$\lambda_i$	: Slip ratio of i-th wheel
$F_{txi}$	: Longitudinal tire force at i-th wheel
$F_{tyi}$	: Lateral tire force at i-th wheel
$F_{tzi}$	: Vertical tire force at i-th wheel
$F_{sxi}$	: Longitudinal internal force acting on a sprung mass
$F_{syi}$	: Lateral internal force acting on a sprung mass
$F_{szi}$	: Vertical internal force acting on a sprung mass
$M_{sxi}$	: Internal moment acting on sprung mass about the roll axis

$M_{szi}$	: Internal moment acting on sprung mass about the yaw axis
$k_s$	: Rotational spring stiffness
$C_d$	: Rotational damping coefficient
$T_{self}$	: Self aligning torque
$\lambda_{max}$	: Maximum slip ratio
$V_{des}$	: Longitudinal desired speed
$y_r$	: Lateral position error
$\varphi_d$	: Desired yaw angle
$F_{x\_des}$	: Total traction force
$M_{z\_des}$	:Yaw moment input
$X_i$	: Desired longitudinal tire force of i-th wheel
$\hat{F}_{txi}$	: Estimated longitudinal tire force of i-th wheel
$\hat{F}_{tzi}$	: Estimated vertical tire force of i-th wheel
$T_{com\_i}$	: Torque command of i-th wheel-in motor

## References

- [1] K. Yi and T. Chung, An Investigation into Differential Braking Strategies for Vehicle Stability Control, IMechE (2003) 217, Part D 1081-1093.
- [2] J. Kang et al, Skid Steering Based Maneuvering of Robotic Vehicle with Articulated Suspension, SAE 2009 World Congress, USA (2009).
- [3] Suresh Golconda, Steering controller for a skid-steered autonomous ground vehicle at varying speed, PhD Thesis, Osmania University, (2005).
- [4] J. T. Economou and R. E. Colyer, Modelling of skid steering and fuzzy logic vehicle ground interaction, Proceedings of the American Control Conference, 0-7803-551 9-9/00, (2000).
- [5] W. E. Dixon, D. M. Dawson, E. Zergeroglu and A. Behal, Nonlinear control of wheeled mobile robots, In Lecture Notes in Control and Information Sciences, 262 Springer-Verlag, London, (2001).
- [6] J. Kang et al, Design and Testing of a Controller for Autonomous Vehicle Path Tracking Using GPS/INS Sensors, IFAC, Proceedings of the 17th World Congress, Korea. (2008) 2093-2098.
- [7] H. Peng, Vehicle Lateral Control for Highway Automation, PhD Thesis, University of California at Berkeley (1992).
- [8] Q. Zhang et al, A Study of Calculation Method of Wheel Angular Acceleration in ABS System, Proceedings of 2004 International Conference on Information Acquisition (2004).
- [9] W. Cho, J. Yoon, S. Yim, B. Koo and K. Yi, Estimation of tire forces for application to vehicle stability control, IEEE Transactions on Vehicular Technology, to be published.
- [10] L. R. Ray, Non-linear tyre force estimation and road friction identification: simulation and experiments, *Automatica* 33 (10) (1997) 1819-1833.
- [11] J. Kang et al, Development and Validation of a Finite Preview Optimal Control-based Human Driver Steering Mode", KSME Spring Conference, Korea (2007) 130-135.
- [12] O. Mokhiamar and M. Abe, Simultaneous Optimal Distribution of Lateral and Longitudinal Tire Forces for the Model Following Control, *ASME Journal of Dynamic Systems*,

*Measurement, and Control*, 126 (2004) 753-763.

- [13] Kenneth R. Buckholtz, Reference input wheel slip tracking using sliding mode control, SAE 2002 World Congress, USA (2002).



**Juyong Kang** received the B.S. and M.S. degrees in mechanical engineering and mechanical design engineering from Hanyang University, Korea, in 2005 and 2007, respectively. Since 2008, he has been a Ph.D. candidate in mechanical and aerospace engineering at Seoul National University, Korea. His research

interest is Autonomous Robot Vehicles.



**Wongun Kim** received the B.S. and M.S. degrees in mechanical engineering and mechanical design engineering from Hanyang University, Korea, in 2005 and 2007, respectively. Since 2008, he has been a Ph.D. candidate in program in automotive engineering at Seoul National University, Korea. His

research interest is Autonomous 6WD/6WS Vehicles.



**Jongseok Lee** received the B.S. and M.S. degrees in mechanical engineering from Pukyong National University, Korea, in 1997 and 1999, respectively. He is working in SAMSUNG TEKWIN in Korea. His research interests are Drive control systems and active safety systems of a ground vehicle.



**Kyongsu Yi** received the B.S. and M.S. degrees in mechanical engineering from Seoul National University, Korea, in 1985 and 1987, respectively, and the Ph.D. degree in mechanical engineering from the University of California, Berkeley, in 1992. Dr. Yi is a Professor at the School of Mechanical and Aero-

space Engineering at Seoul National University, Korea. He currently serves as a member of the editorial boards of the KSME, IJAT and ICROS journals. Dr. Yi's research interests are control systems, driver assistant systems, and active safety systems of a ground vehicle.